# Influence of Atmospheric Pollution on Materials of Culture Heritage. A Physicochemical Study

I. BASSIOTIS , T. AGELAKOPOULOU, S. MARGARITI, V. SIOKOS, E. METAXA, CH. KARAGIANNI, F. ROUBANI-KALANTZOPOULOU*.

School of Chemical Enginnering
National Technical University of Athens
9 Iroon Politechniou, 15780 Zografou
GREECE
roubanif@central.ntua.gr

*Abstract:* - Air pollution influences all aspects of social and economical life nowadays. In order to investigate the impact of air pollution on materials of works of art, the method of Reversed Flow – Inverse Gas Chromatography has been selected. The presence of various atmospheric pollutants is studied on marbles, ceramics, metal oxides (pigments of works of art and building materials) and pieces of authentic sculptures from the Ancient Museums of Kavala and of Filippoi. The method leads to the determination of several physicochemical quantities, which enables the physicochemical characterization of the heterogeneous surfaces of the solids. Moreover, the influence of one or several pollutants (synergistic effect) is examined. The structure, the properties and the behaviour of the materials are examined by X-Ray Diffraction, Scanning Electron Microscopy and Raman Spectroscopy. All the above answer in detail to the questions of where, when and how the influence of gas pollutants on materials of cultural heritage takes place.

*Key-Words:* - Influence of pollutants on works of art, synergistic effect, local physicochemical quantities, RF-IGC.

## 1 Introduction

Air pollution has increased dramatically the last decades. Major sources of air pollution are the exhaust gases from vehicles, power plants and heaters from apartments. Global warming, deterioration of forests, pollution of water basins are some of the sequences. Moreover, an important question arises from the influence of gas pollutants on the surfaces of various monuments and works of art.

A suitable method has been selected in order to study in depth this impact, the so called Reversed Flow – Inverse Gas Chromatography (RF-IGC), studying adsorption and desorption phenomena of gases on solids [1-3]. Several important physicochemical quantities are determined, as local adsorption energy, local adsorption isotherm, local monolayer capacity, density probability function, local adsorption equilibrium concentration and energy from lateral interactions. This simple method has been proved accurate; it emphasizes on solids properties in contrast to classical Gas Chromatography and enables the physicochemical characterization of heterogeneous surfaces. Furthermore, Time Resolved Analysis is achieved,

providing detailed investigation of phenomena and mechanisms [4-7].

The determination of all these physicochemical quantities is based on an appropriate mathematical model.

In this paper the impact of aliphatic hydrocarbons $C_2$-$C_4$ on marbles, ceramics, metal oxides (pigments of works of art and building materials) and pieces of authentic sculptures from the Ancient Museums of Kavala and of Filippoi is investigated. Furthermore, the coexistence of a second pollutant ($O_3$, $SO_2$, $NO_2$) is also studied.

## 2 Mathematical Model

The calculation of all the new physicochemical quantities has been performed using recently published models [2-3].
The main equation remains Eq.(1)

$$H^{1/M} = gc(l^{©}, t) = \sum_{i=1}^{4} A_i \exp(B_i t) \qquad (1)$$

where:
$H$ : height of sample peaks resulting from the flow reversal, cm.

$M$ : response factor of the detector, dimensionless.
$g$ : calibration factor of the detector, cm / mol cm$^{-3}$
$c(l',t)$: measured sampling concentration of the pollutant (eg benzene) at $x = l'$ mol cm$^{-3}$.

The explicit calculation of the adsorption parameters for the gases studied can be carried out in an analogous way to the one described earlier. All parameters refer to the values of $c_y(0,t)$, i.e. the concentration of the gaseous pollutant at y = 0:

$$c_y(0,t) = \frac{vL_1}{D_z} c(l',t) = \frac{vL_1}{gD_z} \sum_{i=1}^{4} A_i \exp(B_i t) \quad (2)$$

where $v$ is the linear velocity of the carrier gas (cm s$^{-1}$) in the sampling column, $L_1$ the length of the diffusion column (cm) and $D_z$ the diffusion coefficient of each hydrocarbon pollutant into the nitrogen carrier gas (cm$^2$ s$^{-1}$). From this, the value of the adsorbed concentration $c_s^*$ is calculated

$$c_s^* = \frac{\alpha_y}{\alpha_s} k_1 \frac{vL_1}{gD_z} \sum_{i=1}^{4} \frac{A_i}{B_i} [\exp(B_i t) - 1] \quad (3)$$

where, the first fraction corresponds to the ratio of the cross sectional area of the void diffusion column (cm$^2$) to the amount of solid adsorbent per unit length of the same column (g cm$^{-1}$),
$k_1$ is the local adsorption coefficient, and the rest of the symbols have been explained after Eq.(2). The local adsorption isotherm is given by

$$\theta_t = \frac{c_s^*}{c_{max}^*} \quad (4)$$

where $c_{max}^*$ is the local monolayer capacity, and $c_s^*$ is given by Eq.(3).

$$c_{max}^* = c_s^* + \frac{\partial c_s^* / \partial c_y}{KRT} \quad (5)$$

Thus, for the $c_{max}^*$ determination the derivative

$$\frac{\partial c_s^*}{\partial c_y}$$

and $KRT$ from Eqs.(6) and (7), respectively, are needed:

$$\frac{\partial c_s^*}{\partial c_y} = \frac{a_y}{a_s} k_1 \frac{\sum_{i=1}^{4} A_i \exp(B_i t)}{\sum_{i=1}^{4} A_i B_i \exp(B_i t)} \quad (6)$$

$$KRT = \frac{gD_z}{vL_1} \left\{ \frac{\sum_{i=1}^{4} A_i B_i^2 \exp(B_i t)}{\left[ \sum_{i=1}^{4} A_i B_i \exp(B_i t) \right]^2} - \frac{1}{\sum_{i=1}^{4} A_i \exp(B_i t)} \right\} \quad (7)$$

In all equations above $A_i$ and $B_i$ are the pre-exponential factors and the exponential coefficients of Eq.(1). The relations for calculating the adsorption energy $\varepsilon$ (kJ/mol) and the modified probability density function $\varphi(\varepsilon)$ from experimental data are given by Eqs 8-9 :

$$\varepsilon = RT \left[ \ln(KRT) - \ln(RT) - \ln K^o \right] \quad (8)$$

$$\varphi(\varepsilon;t) = \theta f(\varepsilon) / c_{max}^* \quad (9)$$

where:

$$f(\varepsilon) = \frac{\partial c_{max}^*}{\partial \varepsilon} = \frac{\partial c_{max}^* / \partial t}{\partial \varepsilon / \partial t} \quad (10)$$

The energy from lateral interactions is given by

$$\beta \theta = \theta z \omega / RT \quad (11)$$

## 3  Experimental Setup

The experimental arrangement is shown in Fig.1 and has been extensively described in [2]. The whole sampling cell is accommodated inside the oven of a gas chromatograph Shimadzu GA-8A, having a temperature control accuracy 1$^o$C. The carrier gas in all cases was nitrogen 99.% from Air Liquide. Thus, a small quantity of gas was injected into the column $L_2$. In the experiments for the synergistic effects of nitrogen dioxide, ozone and sulfur dioxide, this second pollutant was injected through the same column. A typical chromatogram attained is shown in Fig.2.
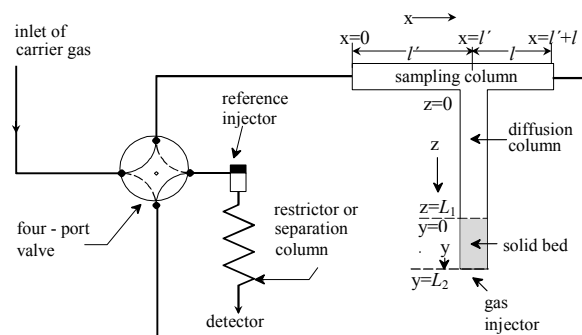
Fig.1, Experimental setup of Reversed Flow-Inverse Gas Chromatography

The systems A/X, B/X and A/B/X are examined, where:
A:    aliphatic hydrocarbons $C_2$-$C_4$, saturated or unsaturated.
B: inorganic gases, $O_3$, $SO_2$, $NO_2$.
X: solid adsorbents, i.e. marbles, metal oxides (building materials and pigments of works of art) as well as samples (sculptures) from the Archeological museums of Kavala and Filippoi.
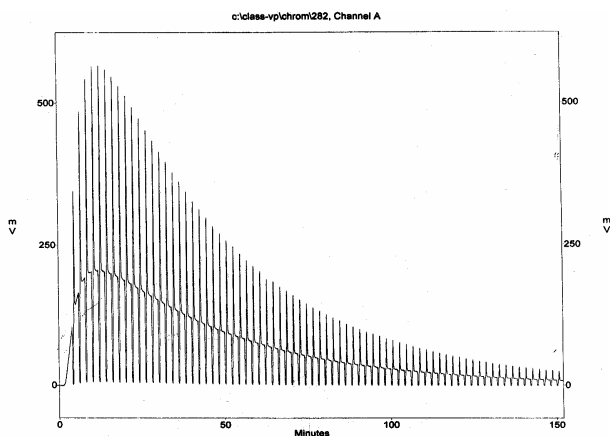
Fig.2, Typical Chromatogram of RF-IGC for the system $C_2H_2$/CaO at 50°C

## 4   Results and Discussion

The local adsorption energy, $\varepsilon$, versus $t$ is depicted in Fig. 3, as well as the local adsorption isotherm, $\theta$, versus $t$ in Fig.4. The curves of every system gas pollutant-solid have analogous shape and their maxima and minima are observed at the same time. The minimum corresponds to the time when the monolayer coverage has finished. This depends on the number of C atoms that the adsorbed gas has in its molecule. At the time where the maximum of the curve $\varepsilon$=f($t$) is occurred, minimum occurs in the diagram of distribution density function $\varphi(\varepsilon;t)$ for the respective system, as it is shown in Fig.6. That is because the probability to find active centres with the maximum energy is very low.
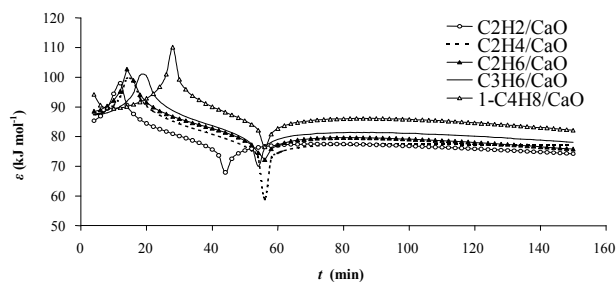
Fig.3, Plots of local adsorption energy, $\varepsilon$, versus $t$ for the systems $C_2H_2$/CaO, $C_2H_4$/CaO, $C_2H_6$/CaO, $C_3H_6$/CaO, 1-$C_4H_8$/CaO at 50°C

Plots of distribution density function, $\varphi(\varepsilon;t)$, versus local adsorption energy, $\varepsilon$, are presented in Fig.5, where the curves have the shape of a normal distribution function (Gauss), the initial in time region (A) and the last in time region (C) to be very close to the central one (B).
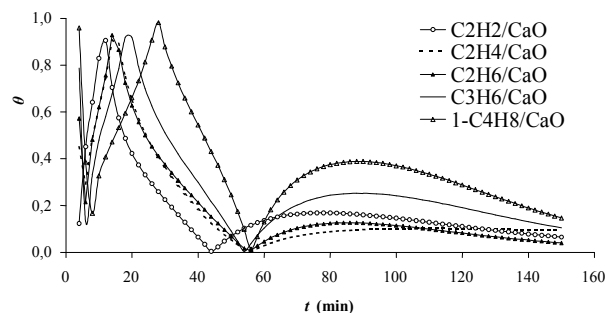
Fig.4, Plots of local adsorption isotherm, $\theta$, versus $t$ for the systems $C_2H_2$/CaO, $C_2H_4$/CaO, $C_2H_6$/CaO, $C_3H_6$/CaO, 1-$C_4H_8$/CaO at 50°C
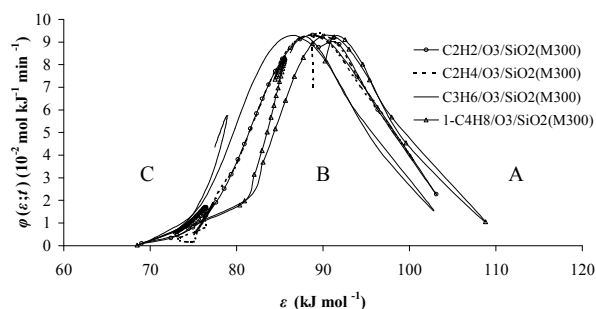
Fig.5, Plots of distribution density function $\varphi(\varepsilon;t)$ versus local adsorption energy, $\varepsilon$, for the systems $C_2H_2$/SiO$_2$/O$_3$/SiO2 (M300), $C_2H_4$/ $O_3$/SiO$_2$ (M300), $C_2H_6$/$O_3$/SiO$_2$ (M300), $C_3H_6$/$O_3$/SiO$_2$ (M300), 1-$C_4H_8$/$O_3$/SiO$_2$ (M300) at 50°C.

On the contrary, the regions A, B, C, are totally different in Fig.6, where the density probability function is plotted versus $t$, which can be explained with the mechanism of Bakaev and Steele [8], attributed to three different kinds of active centers of adsorption. Moreover, the shape of the curves remains almost stable, except for those of the marbles, where two maxima exist and the % fraction of the active centers is much lower.

The results do not change significantly with the presence of $O_3$, but change with the presence of $SO_2$ or $NO_2$. The times of maxima and minima increase from the lower molecular weight of the adsorbed gas to the higher one, under the same experimental conditions. The greater time intervals are attributed to 1-butene and the lower to acetylene. This fact is explained by the respective diffusion coefficients, as lower is the diffusion coefficient as higher is the respective time. A change in % fraction of the region under the third maximum is presented. Furthermore, a different behavior of the solid adsorbents occurs.
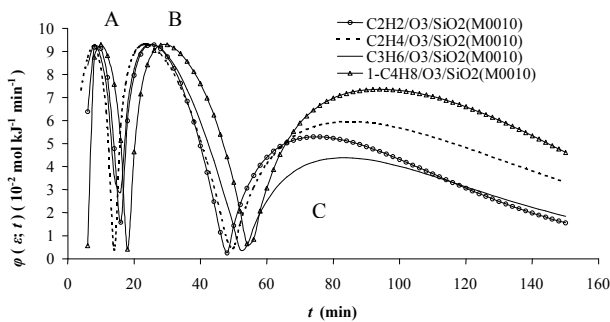


Fig.6, Plots of distribution density function, $\varphi(\varepsilon;t)$ versus $t$ for the systems $C_2H_2/O_3/SiO_2$ (M0010), $C_2H_4/O_3/SiO_2$ (M0010), $C_2H_6/O_3/SiO_2$ (M0010), $C_3H_6/O_3/SiO_2$ (M0010), $1\_C_4H_8/O_3/SiO_2$ (M0010) at $50^{o}C$.

The three maxima and the two minima in Fig.6 occur in the same time with the three maxima and the two minima in the plot of the energy from lateral interactions, $\beta\theta i$, versus $t$ (cf. Fig.7).
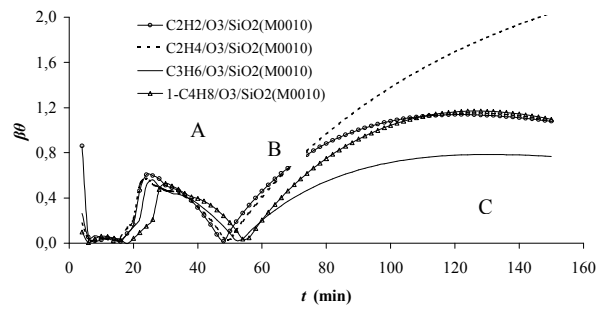


Fig.7, Plot of energy from lateral interactions, $\beta\theta i$, versus $t$ for the systems $C_2H_2/O_3/SiO_2$ (M0010), $C_2H_4/O_3/SiO_2$ (M0010), $C_2H_6/O_3/SiO_2$ (M0010), $C_3H_6/O_3/SiO_2$ (M0010), $1\_C_4H_8/O_3/SiO_2$ (M0010) at $50^{o}C$.

For the plots of local adsorption equilibrium concentration, $c_y$, versus $t$ (cf. Fig. 8) it is observed for all the systems studied that the shape of the curve does not change, the slopes and the maximum values change. This curve comes out from the mathematical model, but also is the same with the so called diffusion band, which comes directly from the experiment. A fact that shows that the results from the experiment and the mathematical model are in total agreement.
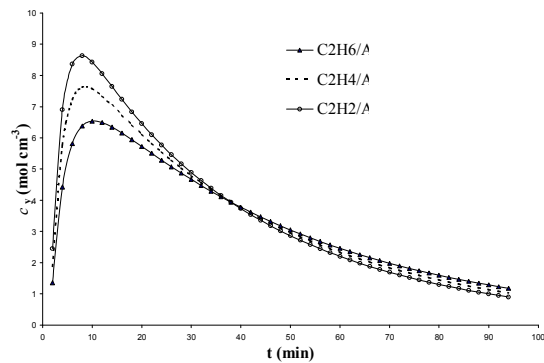


Fig.8, Local adsorption equilibrium concentration, $c_y$, verus $t$ for the systems $C_2H_6$ / Sculpture Λ 291 Museum Kavala, $C_2H_4$ / Sculpture Λ 291 Museum Kavala, $C_2H_2$ / Sculpture Λ 291 Museum Kavala

It is evident the influence of the type of the bond of the adsorbate from the same adsorbent (sculpture), for molecules of the same more or less molecular weights. There is a relationship between the adsorbate and the non adsorbate gas pollutant in equilibrium.
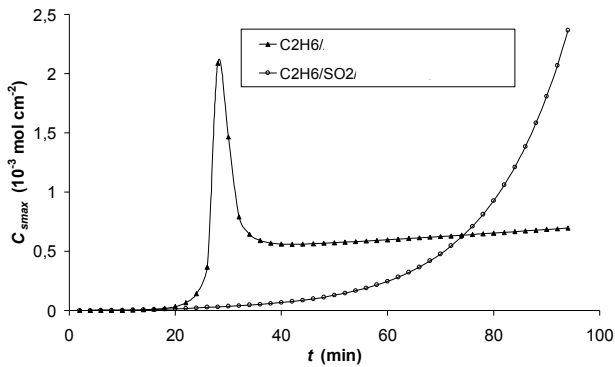
Fig.9, Time Resolved Analysis of local monalyer capacity, $c^*_{max}$, for the systems $C_2H_6$/Sculpture $\Lambda$ 1991 Museum Filippoi, $C_2H_6$/$SO_2$/Sculpture $\Lambda$ 1991 Museum Filippoi.

Regarding the plot of local monolayer capacity, $c^*_{max}$, versus $t$, a different behaviour is observed when $SO_2$ exists (cf. Fig.9). In analogous experiments with the presence of $O_3$, lower values for $c^*_{max}$ are determined, which is attributed that $O_3$ oxidizes the hydrocarbon in gas / homogeneous phase before the adsorption, so lower quantities of gas are detected. An alternative is that $O_3$ acts competitively towards gas pollutant, as it covers active sites on the surface, which leads to lower adsorption of the organic gas.

XRD analysis was performed in the samples of marble and the sculptures from the Archeological Museums of Kavala and Filippoi before and after the injection of the pollutants. It was found that no qualitative change occurred.

Raman analysis was performed in the sample of sculpture of the Archeological Museum of Kavala before and after the influence of the hydrocarbons (cf. Fig.10). Bonds of C-C και C≡C were detected, which is attributed that ethane and acetylene were adsorbed. From the combination of Raman and SEM analysis, $SO_2$ was found, showing that it was adsorbed.
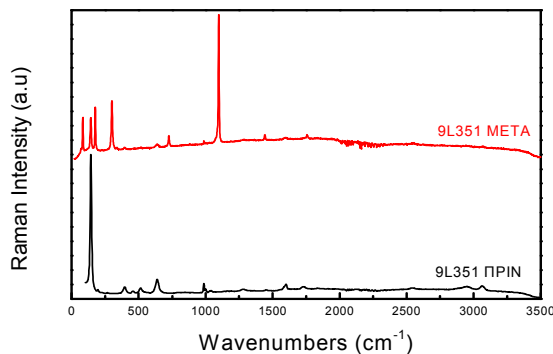


Fig. 10, Raman spectra from a piece of sculpture

from Musuem of Kavala, before (black line) and after (red line) the influence of hydrocarbon.

Fig.11 (a & b) shows the difference between a grain of calcite and dolomite.
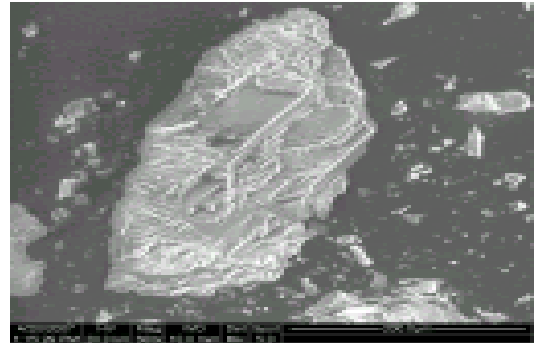


(a)
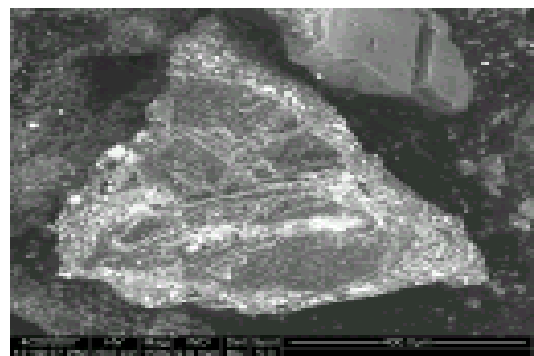


(b)

Fig. 11, SEM images showing the shapes of calcite (a) and dolomite (b).

It is evident that RF-IGC method combined with a suitable mathematical model, provides a valuable tool, in a modern laboratory, in order to investigate the impact of atmospheric pollution on solids. The big difference is that, in this case, all the physicochemical quantities are obtained experimentally and not analytically.

*References:*
[1] X1. N. A. Katsanos, E Iliopoulou, F. Roubani-Kalantzopoulou, E. Kalogirou, Probability

Density Function for Adsorption Energies over Time on Heterogeneous Surfaces by Inverse Gas Chromatography, *Journal of Physical Chemistry B*, Vol. 103, 1999, pp. 10228-10233.

[2] X2. N.A. Katsanos, F. Roubani-Kalantzopoulou, Advances in Physico-chemical Measurements using Inverse Gas Chromatography, *Advances in Chromatography*, Vol. 40, 2000, pp. 231-273.

[3] X3. F. Roubani-Kalantzopoulou, Determination of Isotherms by Gas – Solid Chromatography. Applications, *Journal of Chromatography. A*, Vol. 1037, 2004, pp. 191-221.

[4] X4. E. Metaxa, T. Agelakopoulou., I. Bassiotis , S. Margariti, V. Siokos, F. Roubani – Kalantzopoulou, Time - Resolved Gas Chromatography Applied to Submonolayer Adsorption - Modeling and Experimental Approach, 6th International Symposium on Effects of Surface Heterogeneity in Adsorption and Catalysis on Solids, ISSHAC-6, Zakopane, Poland, 2006, pp. 215.

[5] X5. E. Metaxa, T. Agelakopoulou, I. Bassiotis, S. Margariti, V. Siokos, F. Roubani-Kalantzopoulou, Time–Resolved Gas Chromatography Applied to Submonolayer Adsorption. Modeling and Experimental Approach, *Applied Surface Science*, Vol. 253, 2007, pp. 5841-5845.

[6] X6. T. Agelakopoulou, I. Bassiotis, E. Metaxa, F. Roubani-Kalantzopoulou, Benzene and Toluene Influence with or without Nitrogen Dioxide, *Atmospheric. Environment*, Vol. 41, 2007, pp. 2009-2018.

[7] X7. T. Agelakopoulou, F. Roubani-Kalantzopoulou, Lateral Adsorption Quantities Determination Concerning the Interaction of Aromatic Hydrocarbons with Inorganic Pigments, Colloids & Surfaces. A, Submitted for publication.

[8] X8. V.A. Bakaev, W.A. Steele, Computer Simulation of the Adsorption of Argon on the Surface of Titanium Oxide. 1. Crystalline Rutile, *Langmuir*, Vol. 8, 1992, pp. 1372-1378.